American Journal of Biomedical Sciences
ISSN: 1937-9080
nwpii.com/ajbms

In Vitro Transformation of Sol-gel Derived Bioactive Glass from Sand

Luqman A. Adams[1*] and Enobong R. Essien[2]

[1] Department of Chemistry, University of Lagos, Nigeria
[2] Department of Chemical Sciences, Bells University of Technology, Nigeria
[*]**Corresponding Author**
Luqman A. Adams
Department of Chemistry
University of Lagos
Nigeria
Email: ladams@unilag.edu.ng.

Received: 01 July 2015; | Revised: 23 November 2015; | Accepted: 02 December 2015

Abstract

A Bioactive glass in the quaternary system SiO_2–Na_2O–CaO–P_2O_5 was prepared from sand as precursor in place of alkoxysilanes such as tetraethyl orthosilicate (TEOS) and tetramethyl orthosilicate (TMOS). Sodium metasilicate extracted from the sand was processed to a gel via the sol-gel technique. The gel, after aging was dried at lower temperatures before sintering at 950 ^oC for 3 h to form $Na_2Ca_2Si_3O_9$ crystals for enhanced mechanical property. The glass monolith was then subjected to standard *in vitro* bioactivity study in simulated body fluid (SBF) over 0-21 days. Characterization of the samples before and after immersion in SBF were performed using mechanical tester, scanning electron microscopy (SEM), energy dispersive X-ray (EDX), X-ray diffraction and Fourier transform infrared (FTIR) to evaluate compression strength, morphology, composition, diffraction patterns and chemical bonding respectively. The compression strength of the glass was 1.77 Mpa. The major crystalline phase was $Na_2Ca_2Si_3O_9$ which, however, transformed to an amorphous phase in SBF while forming hydroxyapatite (HA) and hydroxycarbonate apatite (HCA). The material may be a useful candidate in the regeneration of trabecular bones.

Keywords: Silica source; $Na_2Ca_2Si_3O_9$; Compression strength; Trabecular bone; Hydroxycarbonate apatite.

1. Introduction

Synthetic bioactive glasses are unique for eliciting bone-bonding reactions when used *in vivo* and *in vitro* making them attractive materials for restoration of damaged or diseased tissues and bones. Consequently, effort is ongoing towards developing suitable glass materials tailored to achieve the main features for ideal bone tissue engineering scaffolds [1-6]. Biological compatibility, appropriate mechanical strength and osteointegration properties are vital for optimal performance which should culminate in formation of hydroxycarbonated apatite HCA [6-9].

While formation of HCA layer is considered to be a useful step in bone regeneration process, other key factors include: critical concentrations

of dissolution products from silicate-based bioactive glasses and gene expression [10-13].

Glasses based on Hench's 45S5 composition [14-16] have been widely studied for their mechanical properties and concomitant *in vivo* and *in vitro* bioactivity in relation to surface reactivity in body fluids. There are still challenges regarding mechanical properties, biodegradation and bioactivity [17-19].

For glasses containing Na_2O in the composition, sintering leads to the formation of $Na_2Ca_2Si_3O_9$ crystalline phase which significantly improves their mechanical strength, while transforming to amorphous hydroxyapatite (HA) in SBF [6,20-23]. Significantly, those efforts have utilised tetraethyl orthosilicate [TEOS] as precursor [6,8,20-22]. Our aim in this work, therefore, is to use sand as a cheap silica source to obtain bioactive glass in the quaternary system SiO_2–Na_2O–CaO–P_2O_5 and evaluate the transformation of the crystalline $Na_2Ca_2Si_3O_9$ phase formed in simulated body fluid.

2. Materials and methods

2.1. Materials

The sand used as starting material was obtained from Ifo in Ogun State, South-West Nigeria and had a composition shown elsewhere [23]. Analytical grade reagents were used as obtained: $NaNO_3$ (Sigma-Aldrich, 99%), $Ca(NO_3)_2{\cdot}4H_2O$ (Loba Chemicals, 98%), H_3PO_4 (Sigma-Aldrich, 85%) and HNO_3 (Riedel-DeHaën, 60%) to synthesize the bioactive glass. NaCl, $NaHCO_3$, KCl, $K_2HPO_4{\cdot}3H_2O$, $MgCl_2{\cdot}6H_2O$, $CaCl_2$, trishydroxymethyl aminomethane [Tris-buffer, $(CH_2OH)_3CNH_2$] and 1M HCl used to prepare SBF were purchased from Sigma-Aldrich.

2.2. Preparation of bioactive glass

The procedure for preparing the glass with composition (mol %) 46.99 SiO_2–24.36 Na_2O–25.50 CaO–3.15 P_2O_5 is a modification of Chen *et al.*'s [22] method of synthesizing sol-gel Bioglass® 45S5. Briefly, sodium metasilicate, obtained from the sand through a procedure reported previously [23], was added slowly to stirred 0.05M HNO_3 and allowed for 1 h to complete the hydrolysis. Afterwards, to the mixture, $NaNO_3$, H_3PO_4 and $Ca(NO_3)_2{\cdot}4H_2O$ were added sequentially for which molar ratio of water to all the four reagents were fixed at 20. Each reagent was allowed to react for 45 min after each addition. Thereafter, the final mixture was stirred for additional 1 h before transferring the resulting sol into teflon moulds and kept at room temperature for 72 h. The gel obtained was heated at as follows; 70°C for 72 h, 130°C for 42 h, 700°C for 2 h and 950°C for 3 h to age, dry, stabilize and sinter respectively. The heating and cooling rate was maintained at 5°C/min.

2.3. Characterization

The density ρ_{glass} of the bioactive glass was determined from the mass and dimensions of the sintered body. The porosity *P* was calculated by

$$P = \left(1 - \frac{\rho_{glass}}{\rho_s}\right) \times 100 \qquad (1)$$

where density ρ_s = 2.7 g/cm^3 is the theoretical density of 45S5 Bioglass® [24].

The microstructure of the glass was characterized in a EVO/MAIO scanning electron microscope (SEM) equipped with energy dispersive X-ray analyzer (EDX) before and after immersion in simulated body fluid (SBF) for a maximum of 21 days. The samples were carbon-coated and observed at an accelerating voltage of 15 kV.

Samples were characterized using X-ray diffraction (XRD) analysis after sintering and after each immersion experiment in SBF to investigate the glass phases present. The samples were first ground to powder, then 0.1 g of powder was measured in a PANalytical Empyrean X ray diffractometer using CuKα radiation source of wavelength (λ) = 0.154056 nm operated at 40 kV and 40 mA to obtain the diffraction patterns in the 2θ range from 5° - 90°.

Fourier transform infrared (FTIR) spectroscopy was performed in a Shimadzu 8400S spectrometer with wavenumber range of 4000-400 cm^{-1} employing KBr pellets in a reflectance mode with a 4 cm^{-1} resolution to

monitor the nature of chemical bonds present in the samples.

2.4. Measurement of mechanical Strength

The compression strength of the sintered bioactive glass was measured using a Testometric OL11 INR (Lancashire, England) mechanical tester at crosshead speed of 0.5 mm/min. The samples were cylindrical in shape with dimensions 12 mm x 24 mm (diameter x height). During the compression test, the load was applied until densification commenced. The compression strength was determined using the relation:

$$\sigma_c = F/\pi r^2 \quad (2)$$

where σ_c is the compression strength, F is the applied load at failure and r is the sample radius.

2.5. In vitro bioactivity test in simulated body fluid

Assessment of bone bonding ability was performed using the standard *in vitro* procedure [25]. The acellular simulated body fluid (SBF) was prepared using analytical grade reagents: NaCl, $NaHCO_3$, KCl, $K_2HPO_4 \cdot 3H_2O$, $MgCl_2 \cdot 6H_2O$, $CaCl_2$, trishydroxymethyl aminomethane [Tris-buffer, $(CH_2OH)_3CNH_2$] and 1M HCl with ions concentrations shown in Table 1. Samples were immersed in the SBF solution at a concentration of 0.01 g/ml in clean sterilised plastic bottles, which were initially washed using HCl and deionized water. The bottles were placed inside a thermostated incubator at a temperature of 36.5 ^oC at an initial pH of 7.4. The SBF solutions were not refreshed throughout the period of immersion to monitor pH of the solution daily for 14 days using a pH meter (Hanna, HI96107). The samples were extracted from the SBF solution after 7, 14 and 21 days respectively, rinsed with deionized water and left to dry at ambient temperature in a desiccator. Formation of apatite layer on the glass surface was monitored by SEM, EDX, XRD and FTIR.

Table 1: Ion concentrations (mM) in human plasma in comparison with SBF

Ion	Na^+	K^+	Mg^{2+}	Ca^{2+}	Cl^-	HCO_3^-	HPO_4^{2-}	SO_4^{2-}
SBF	142.0	5.0	1.5	2.5	147.8	4.2	1.0	0.5
Human Plasma	142.0	5.0	1.5	2.5	103.0	27.0	1.0	0.5

3. Results and discussion

3.1. Mechanical strength of the glass

The force-deflection curve obtained from compression test performed on the sintered sample is shown in Figure 1. As observed, four major stages are visible. In the first stage, A, the material maintains a positive slope until a maximum stress is reached, then decreases temporarily due to cracking of the pore struts and closing up of the micropores, stage B. This regime is followed by stage C, where the force-deflection curve rises again as material shows ability to bear higher load due to densification of the pores as more stress is applied on the material [21]. Finally, the material collapses completely under maximum stress, which is in agreement with general findings on the strength value of porous ceramics [8]. The glass under this study exhibited a compression strength of 1.77 MPa and a porosity of 77 %. This result is comparable to the compression strength of spongy bone (not the strut) which is in the range of 0.2–4 MPa [26]. Mechanical strength of spongy or trabecular bone is in the range 0.1 – 16 Mpa, hence this material may find useful application as scaffold for trabecular bone [26,27].

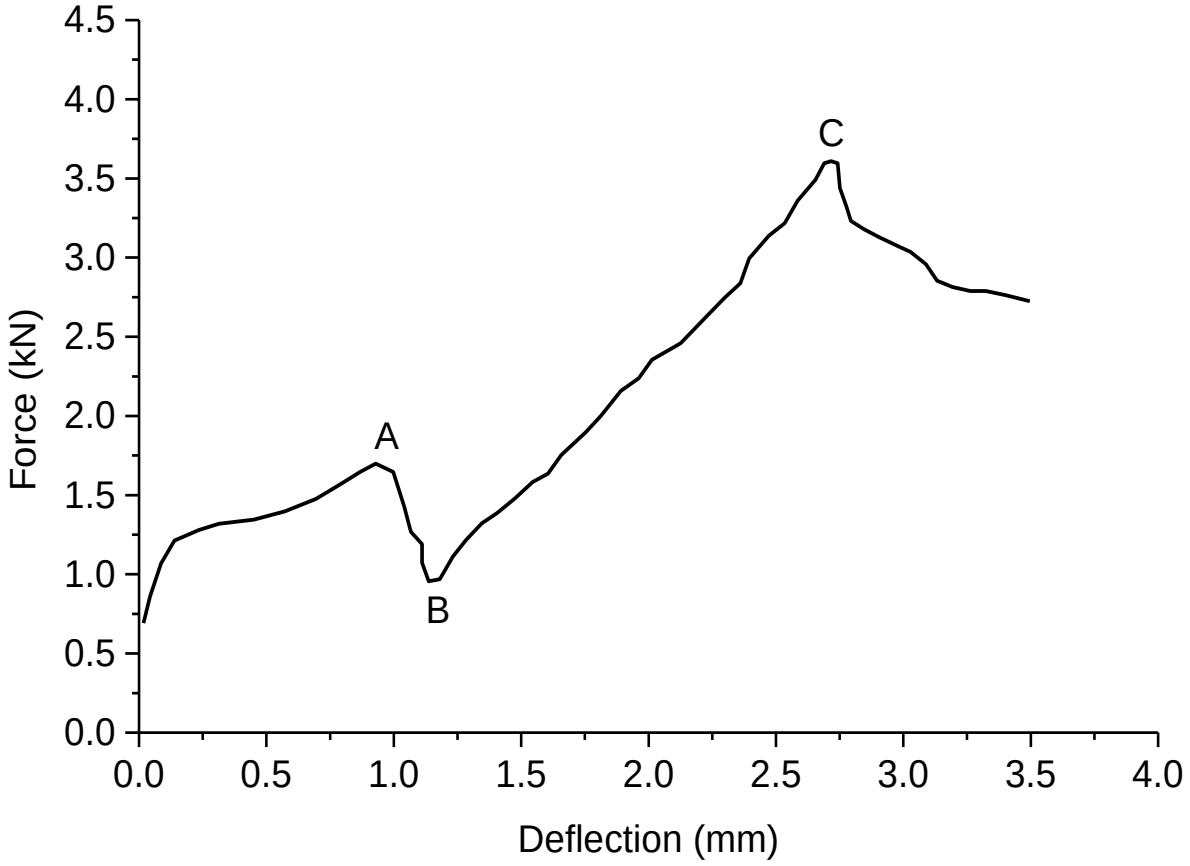

Figure 1. A four-stage force-deflection curve of the bioactive glass sintered at 950 ^{o}C for 3 hours with compression strength of 1.77 MPa.

3.2. Morphology of glass

The SEM micrographs depicting the morphology of the glass before and after immersion in SBF are presented in Figure 2. After sintering, the glass surface, as seen in Figure 2(a), contains plate-like particles ranging from 1.67–3.55 μm which appear to completely cover the surface of the glass providing large surface area and surface roughness with few visible micropores. The large surface area and rough texture are crucial to promote absorption of biological metabolites as well as attachment and proliferation of bone progenitor cell on the material [28-30]. The shape and arrangement of the glass particles suggests good densification of the material, which is important in maximizing the glass mechanical strength. The EDX spectrum indicates the presence of all the chemical components in the various percentages as prepared.

After immersion in SBF for 7 days, tiny balls of HA are seen on the surface of the glass with few agglomerates, Figure 2 (b). As observed in the micrograph, the HA does not completely cover the glass surface leaving exposed areas. This is confirmed by the EDX which could still detect the presence of Si, but there is increase in the concentration of Ca and P due to formation of HA. As immersion period in SBF reached 14 days, the population of HA on the surface of the glass increased and became denser as observed in Figure 2(c). Accordingly, the EDX records low concentration for Si, while P increases further due to increase apatite deposition. After 21 days of immersion in SBF, a thick apatite layer is seen in Figure 2(d) covering the glass surface to the extent that low Si detection is observed in the

EDX. Furthermore, the concentration of P increased during this period resulting in a Ca/P atomic ratio of 1.70, which is close to the stoichiometric ratio of Ca/P of 1.67 in HA. Emergence of a small carbon peak is also visible in the EDX spectra after immersion for 21 days, which is an indication of the formation of HCA. The presence of Mg and Cl are also noticed in the EDX spectra, which can be attributed to insufficient rinse during extraction of the glass from the SBF solution after the various immersion periods.

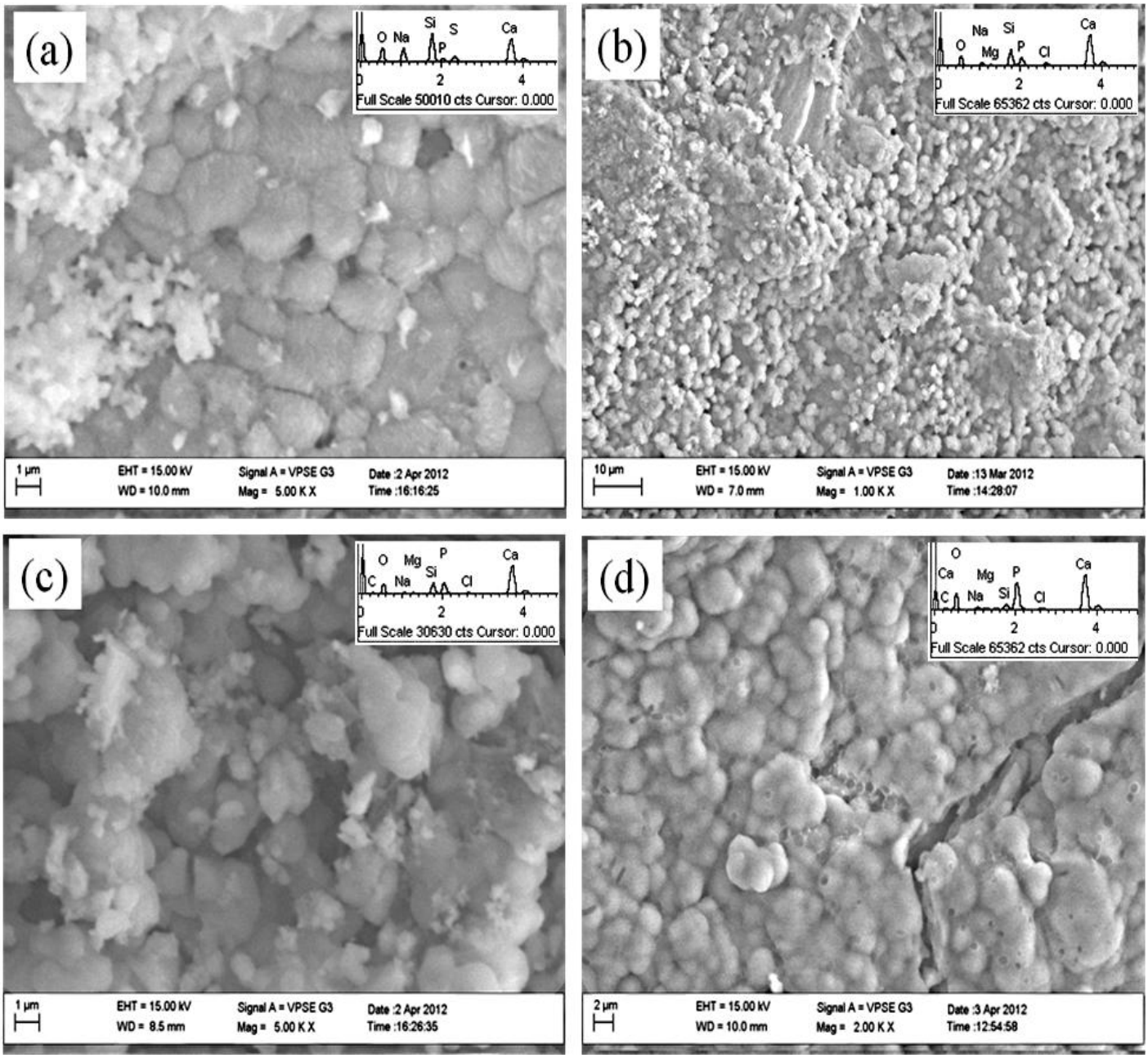

Figure 2. SEM micrographs with EDX insets showing the morphology of the glass before immersion in SBF (a) and after immersion for 7 days (b), 14 days (c) and 21 days showing the growth of apatite.

3.3. Diffraction patterns

The X-ray spectra of the glass are shown in Figure 3. After sintering, the diffraction pattern contains sharp peaks which is identified as $Na_2Ca_2Si_3O_9$ according to the standard PDF #22.1455 [21] and similar to those reported using TEOS for 45S5 Bioglass® at sintering temperature of 1000 ^oC for 2 hours [22,31]. Improved mechanical properties of Na-containing glasses is attributed to the presence of $Na_2Ca_2Si_3O_9$ formed during sintering [18,21]. Thus, the plate-like microstructure observed earlier in Figure 2(a) and the mechanical strength of the glass could be as a result of the presence of this phase.

After soaking in SBF for 7-14 days, Figure 3(b-d) show HA peaks which match the standard PDF file, JCPDS #9-0432 at 2θ 28.9^o, 2θ 31.7^o, 2θ 33.9^o, 2θ 39.8^o and 46.7^o corresponding to the (h k f) planes at 210, 112, 300, 310 and 222 respectively [32,33]. It is also observed that the glass transformed to nearly amorphous phase after 14 days of immersion. After 21 days most of the $Na_2Ca_2Si_3O_9$ peaks had almost completely disappeared, the glass has become more amorphous, the HA peaks at 2θ 28.9^o and 2θ 39.8^o become sharper signalling the formation of crystalline HCA. This phase transformation is significant as the mechanically strong $Na_2Ca_2Si_3O_9$ crystalline structure is able to transform to amorphous, an indication that the glass is biodegradable in biological environments [18]. Hence this transformation corroborates previous findings [21,22,34,35] that the two normally irreconcilable properties: mechanical competence and biodegradability can be combined in a single scaffold for clinical application.

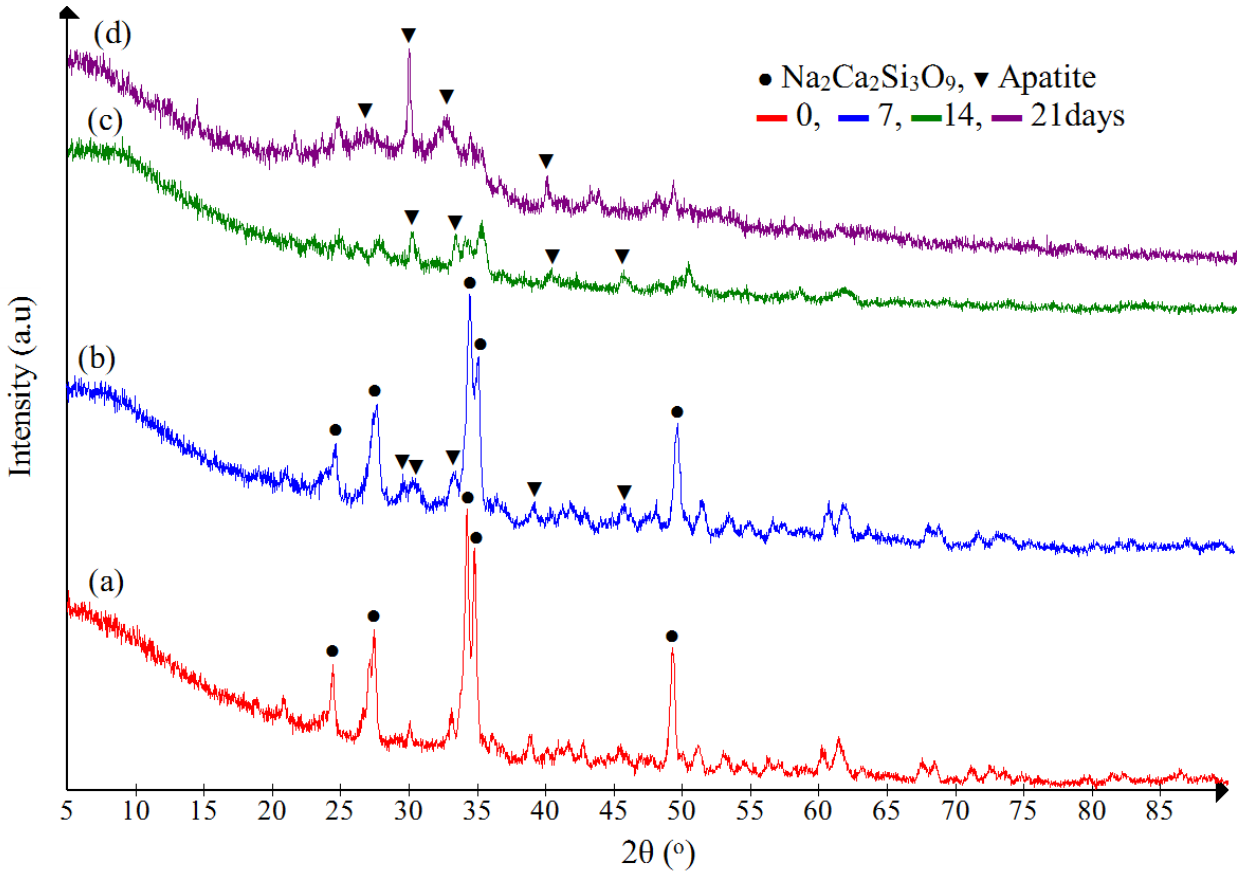

Figure 3. XRD spectra of the glass before immersion in SBF (a) and after immersion in SBF (b)-(d) showing phase transformation from crystalline to amorphous phase and formation of apatite.

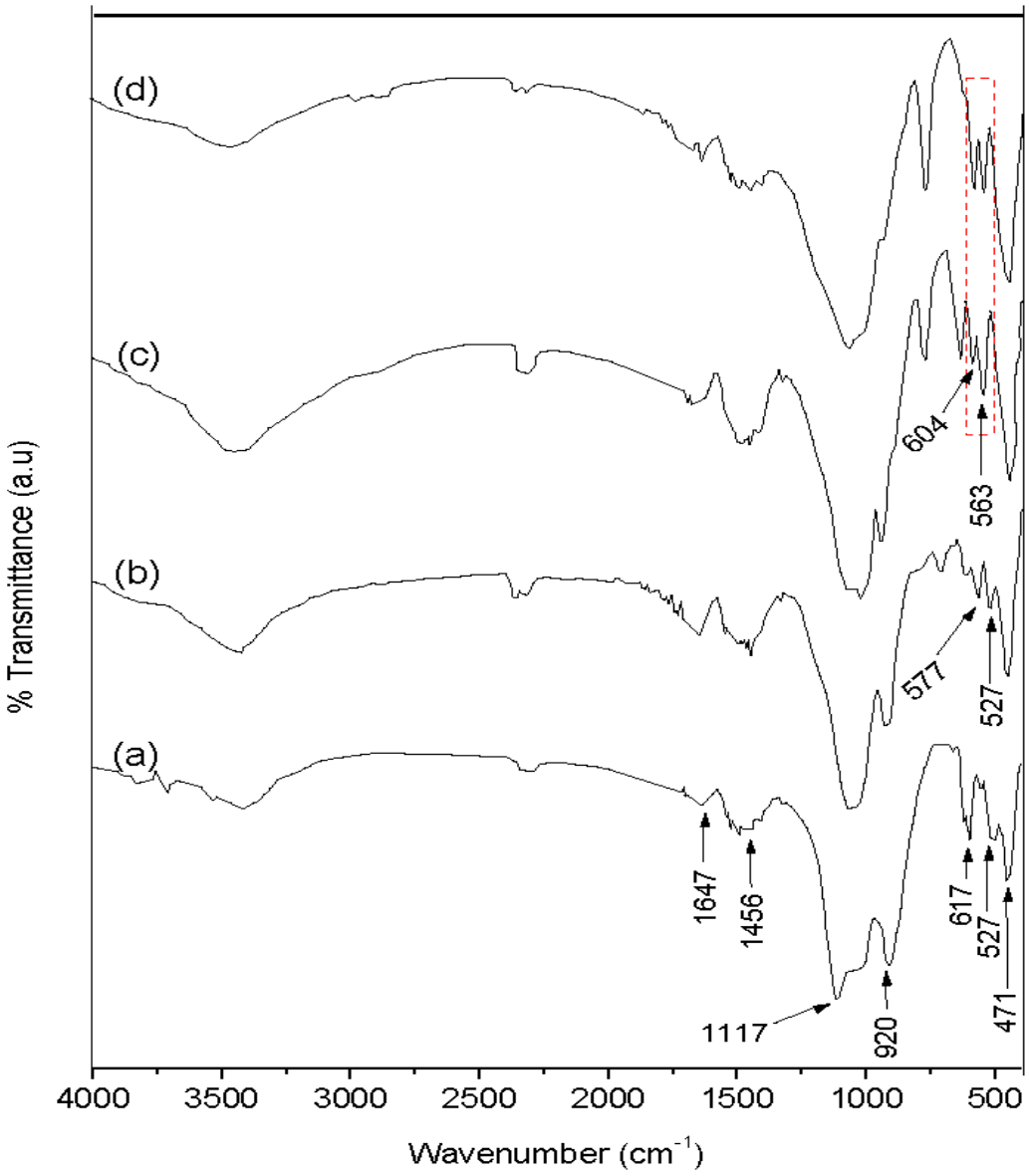

Figure 4. FTIR spectra of the glass before (a) and after immersion in SBF (b)-(d) showing apatite peaks. Red rectangular doted lines represent similar absorption modes.

3.4. FTIR assessment of bonds

The FTIR spectra of the bioactive glass before and after immersion in SBF are shown in Figure 4. As observed before immersion in SBF, Figure 4(a), there are prominent peaks at 3447, 1647, 1456, 1117, 920, 617, 527 and 471 cm^{-1}. The broad band between 3300 – 3800 cm^{-1} centred at 3447 cm^{-1} is attributed to the presence of OH groups, which is further confirmed by the presence of water absorbed band around 1647 cm^{-1}. The band around 1456 cm^{-1} is attributed to the absorption of carbonate group (v_3), while the sharp peak at 1117 and 920 cm^{-1} are associated with Si–O–Si vibrational modes [35]. The peak at 617 and 527 cm^{-1} are due to the crystalline phase in the sample [22], and thus confirms the crystalline $Na_2Ca_2Si_3O_9$ earlier identified by the XRD result (Figure 3). The peak at 471 cm^{-1} is assigned to Si–O–Si bending vibrations. After 7 days, Figure 4(b), the peak at 1456 cm^{-1} becomes more intense, while a new peak emerges at 577 cm^{-1}, considered for P–O bending mode, which is characteristic of HA. The peak at 577 cm^{-1} splits into two modes at 604 and 569 cm^{-1} after 14 days

as shown in Figure 4(c). This is characteristic of apatite crystalline phase [36], suggesting the incorporation of CO_3^{2-} from the SBF solution into HA on the glass surface to form HCA. As immersion days increased to 21, Figure 4(d), the twin peaks at 604 and 563 cm^{-1} become more intense due to increase in density of HCA on the surface of the glass. This therefore confirms the EDX result in Figure 2(d) which showed the appearance of a small peak of C attributed to HCA formation.

3.5. Reactivity of the glass in SBF

The reactivity of the glass evaluated from pH changes in SBF for the first 14 days is presented in Figure 5. There is a steep rise in pH from the initial 7.4 to 8.6 during the first 4 days, which shows the ability of the glass to exchange alkali and alkaline earth ions (Na^+ and Ca^{2+}) rapidly with H^+ or H_3O^+ ions in the SBF. This is in agreement with the first stage of the reaction of bioactive glasses in biological fluids [37] and also signifies the degradation capacity of the glass. After 4 days the pH increases slowly until 6 days because part of the released Ca from the glass is used to form $CaO–P_2O_5$, thus decreasing the release rate. Consequently HA precipitation occurred on the glass surface as shown earlier (Figure 2(b)). As the soaking time reached 7 days the pH increase slowed further as more Ca is withdrawn from the SBF solution to develop more HA layers on the surface of the glass, confirming the increase in density of HA (Figure 2(c)). Finally, the pH reaches a saturated value of 9.3 after 13 days without increasing any further due to crystallization of HCA, whose mechanism is explained elsewhere [38]. Formation of HCA had earlier been identified from the results of EDX, XRD and FTIR in Figures 2(d), 3(d) and 4(d) respectively.

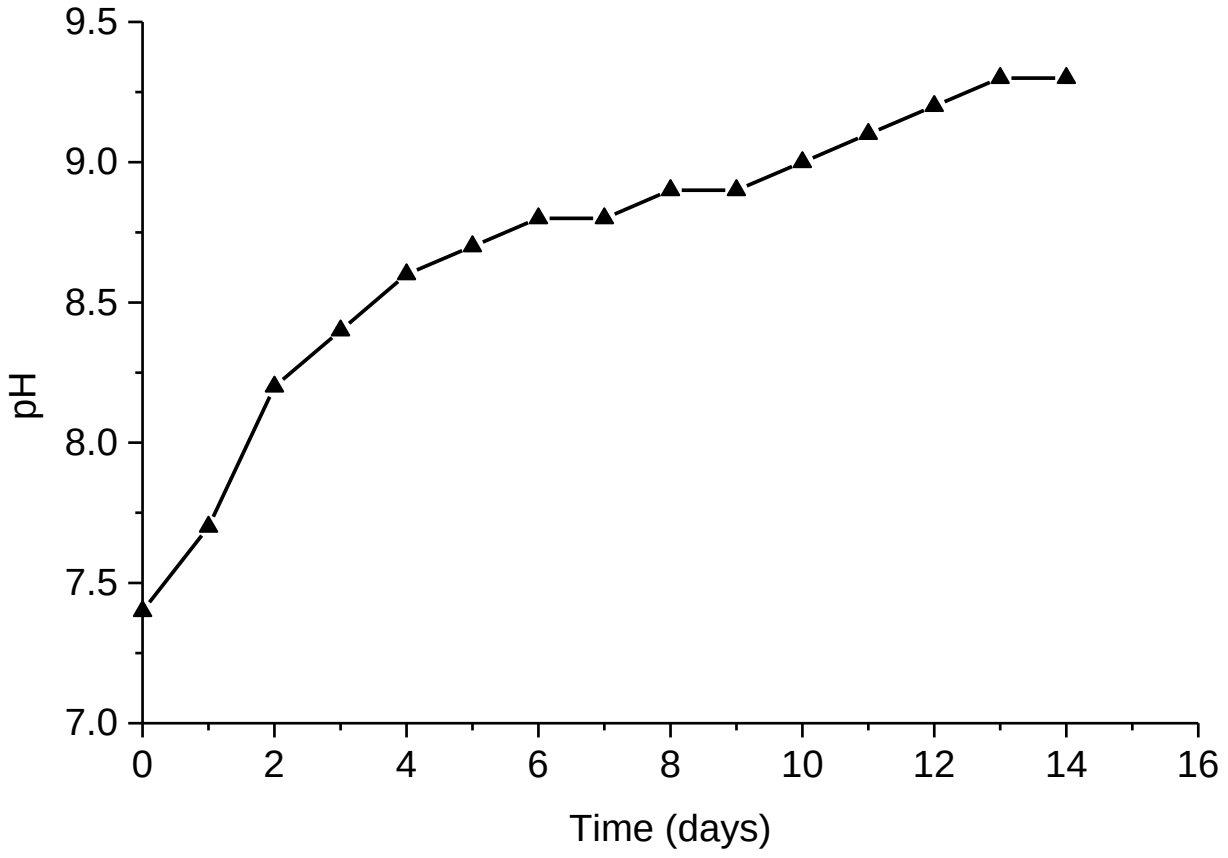

Figure 5. pH changes of the glass for the first 14 days of immersion in SBF.

4. Conclusions

A highly bioactive SiO_2–Na_2O–CaO–P_2O_5 formed using sand as starting material and sintered at 950 ^oC for 3 h gave a compression strength of 1.77 Mpa. The mechanical properties was attributed to proper densification and the presence of $Na_2Ca_2Si_3O_9$ crystalline phase. When immersed in SBF, HA and HCA were identified in the material while the crystalline $Na_2Ca_2Si_3O_9$ transformed to amorphous phase. The mechanical properties and transformation of the glass from crystalline to amorphous within 14 days in SBF indicates degradability and is an important property required to serve as scaffold for tissue engineering of trabecular bone. Furthermore the use of sand as cheap starting material instead of TEOS for this type of study could enhance commercialization of glasses in the SiO_2–Na_2O–CaO–P_2O_5 system.

Acknowledgements

The authors express their gratitude to Sheda Science and Technology Complex (SHESTCO), Abuja and Redeemers University (RUN), Ede, Nigeria, for the SEM/EDX and FTIR Characterization of samples from this work.

References

1. Rezwan, K.; Chen, Q. Z.; Blaker, J. J.; Boccaccini, A. R. Biodegradable and bioactive porous polymer/inorganic composite scaffolds for bone tissue engineering, Biomaterials 2006, 27(18), 3413-3431. DOI: 10.1016/j.biomaterials.2006.01.039
2. Vitale-Brovarone, C.; Miola, M.; Balagna, C.; Verné, E. 3D-glass-ceramic scaffolds with antibacterial properties for bone grafting, Chem. Eng. J. 2008, 137(1), 129-136. DOI: 10.1016/j.cej.2007.07.083
3. Karageorgiou, V.; Kaplan, D. Porosity of 3D biomaterial scaffolds and osteogenesis, Biomaterials 2005, 26(27), 5474-5491. DOI: 10.1016/j.biomaterials.2005.02.002
4. Smith, I. O.; Ren, F.; Baumann, M. J.; Case, E. D. Confocal laser scanning microscopy as a tool for imaging cancellous bone, J. Biomed. Mater. Res. B Appl. Biomater. 2006, 79(1), 85-92. DOI: 10.1002/jbm.b.30529
5. Woodward, J. R.; Hilldore, A. J.; Lan, S. K.; Park, C. J.; Morgan, A.W.; Eurell, J. A.;Clark, S. G.; Wheeler, M. B.; Jamison, R. D.; Wagoner Johnson, A.J. The mechanical properties and osteoconductivity of hydroxyapatite bone scaffolds with multi-scale porosity, Biomaterials 2007, 28(1), 45-54. DOI: 10.1016/j.biomaterials.2006.08.021
6. Vitale-Brovarone, C.; Baino, F.; Verné, E. High strength bioactive glass-ceramic scaffolds for bone regeneration, J. Mater. Sci. Mater. Med. 2009, 20(2), 643-653. DOI: 10.1007/s10856-008-3605-0
7. Hench, L. L. Bioceramics, J. Am. Ceram. Soc. 1998, 81(7), 1705-1728. DOI: 10.1111/j.1151-2916.1998.tb02540.x
8. Peitl, O.; LaTorre, G. P.; Hench, L. L. Effect of crystallization on apatite-layer formation of bioactive glass 45S5, J. Biomed. Mater. Res. 1996, 30(4), 509-514. DOI: 10.1002/(SICI)1097-4636(199604)30:4<509::AID-JBM9>3.0.CO;2-T
9. Aly, AF.; Eldelsouky, AS.; Eid, K. A. M. Evaluation, characterization of ceramic scaffold and nano-gold loaded ceramic scaffold for bone tissure engineering, Am. J. Biomed. Sci. 2012, 4(4), 316-326. DOI: 10.5099/aj120400316
10. Xynos, I. D.; Edgar, A. J.; Buttery, L. D. K.; Hench, L. L.; Polak, J. M. Gene- expression profiling of human osteoblasts following treatment with the ionic products of Bioglass® 45S5 dissolution, J. Biomed. Mater. Res. 2001, 55(2), 151-157. DOI: 10.1002/1097-4636(200105)55:2<151::AID-JBM1001>3.0.CO;2-D
11. Xynos, I. D.; Hukkanen, M. V. J.; Batten, J. J.; Buttery, L. D.; Hench, L. L.; Polak, J. M.

Bioglass® 45S5 stimulates osteoblast turnover and enhances bone formation in vitro: Implications and applications for bone tissue engineering, Calcif. Tissue Int. (2000), 67(4), 321-329. DOI: 10.1007/s002230001134

12. Hench, L. L. Genetic design of bioactive glass, J. Eur. Ceram. Soc. 2009, 29(7), 1257-1265. DOI: 10.1016/j.jeurceramsoc.2008.08.002

13. Jell, G.; Stevens, M. M. Gene activation by bioactive glasses, J. Mater. Sci. Mater. Med. 2006, 17(11), 997-1002. DOI: 10.1007/s10856-006-0435-9

14 Hench, L. L. Abstracts of Papers of the American Chemical Society, vol. 173, 1977, p. 10.

15. Hench, L. L.; Pantano, C. G.; Buscemi, P. J.; Greenspan, D. C. Analysis of bioglass fixation of hip prosthesis, J. Biomed. Mater. Res. 1977, 11(2), 267-282. DOI: 10.1002/jbm.820110211

16. Hench, L. L.; Paschall, H. F.; Paschall, M.; McVey, J. Histological responses at bioglass and bioglass–ceramic interfaces, Am. Ceram. Soc. Bull. 1973, 52(4), 432-432.

17. Boccaccini, A. R. Ceramics, Hench, L. L., Jones J. R. Ed.; Woodhead Publishing Limited CRC Press, 2005; pp 26-36.

18. Boccaccini, A. R.; Chen, Q.; Lefebvre, L.; Gremillard, L.; Chevalier, J. Sintering, crystallisation and biodegradation behaviour of Bioglass-derived glass-ceramics, Faraday Discuss. 2007, 136, 27-44. DOI: 10.1039/b616539g

19. Thompson, I. D.; Hench, L. L. Mechanical properties of bioactive glasses, glass-ceramics and composites, Proc. Inst. Mech. Eng. Part H-J. Eng. Med. 1998, 212(2),127-136. DOI: 10.1243/0954411981533908

20. Du, R.; Chang, J. Preparation and characterization of bioactive sol-gel-derived $Na_2Ca_2Si_3O_9$, J. Mater. Sci. Mater. Med. 2004, 15(12), 1285-1289. DOI: 10.1007/s10856-004-5736-2

21. Chen, Q. Z.; Thompson, I. D.; Boccaccini, A. R. 45S5 Bioglasss-derived glass-ceramic scaffolds for bone tissue engineering, Biomaterials 2006, 27(11), 2414-2425. DOI: 10.1016/j.biomaterials.2005.11.025

22. Chen, Q.-Z.; Yuan, L. Y.; Jin, L.-Y.; Quinn, J. M. W.; Komesaroff, P. A. A new sol-gel process for producing Na2O-containing bioactive glass ceramics, Acta Biomater. 2010, 6(10), 4143-4153. DOI: 10.1016/j.actbio.2010.04.022

23. Essien, E. R.; Adams, L. A.; Shaibu, R. O.; Olasupo, I. A.; Aderemi, O. Economic route to sodium-containing silicate bioactive glass scaffold, Open J. Regen. Med. 2012, 1(3), 33-40. DOI: 10.4236/ojrm.2012.13006

24. Cao, W.; Hench, L. L. Bioactive materials, Ceram. Int. 1996, 22(6), 493-507. DOI: 10.1016/0272-8842(95)00126-3

25. Kokubo, T.; Takadama, H. How useful is SBF in predicting in vivo bone bioactivity? Biomaterials 2006, 27(15), 2907-2915. DOI: 10.1016/j.biomaterials.2006.01.017

26. Jones, J. R.; Lee, P. D.; Hench L. L, Hierarchical porous materials for tissue engineering, Phil. Trans. R. Soc. A. 2006, 364(1838), 263-281. DOI: 10.1098/rsta.2005.1689

27. Wu, Y. Z.; Hill, R. G.; Yue, S.; Nightingale, D.; Lee, P. D. Jones, J. R Melt-derived bioactive glass scaffolds produced by a gel-cast foaming technique, Acta Biomater. 2011, 7(4), 1807-1816. DOI: 10.1016/j.actbio.2010.11.041

28. Deligianni, D. D.; Katsala, N. D.; Koutsoukos, P. G.; Missirlis, Y. F. Effect of surface roughness of hydroxyapatite on human bone marrow cell adhesion, proliferation, differentiation and detachment strength, Biomaterials 2001, 22(1), 87-96. DOI: 10.1016/S0142-9612(00)00174-5

29. Hench, L. L. Sol-gel materials for bioceramic applications, Curr. Opin. Solid State Mater. 1997, 2(5), 604-610. DOI: 10.1016/S1359-0286(97)80053-8

30. Eid, K.; Eldesouky, A.; Fahmy, A.; Shahat, A.; AbdElaal, R. Calcium phosphate loaded

with platinum nanoparticles for bone allograft, Am. J. Biomed. Sci. 2013, 5(4), 242-249. DOI: 10.5099/aj130400242

31. Chen, Q.-Z.; Thouas, G. A. Fabrication and characterization of sol–gel derived 45S5 Bioglass–ceramic scaffolds, Acta Biomater. 2011, 7(10), 3616-3626. DOI: 10.1016/j.actbio.2011.06.005
32. Lin, K. S. K.; Yao-Hung, T.; Mou, Y.; Yu-Chuan, H.; China-Min, Y.; Chan, J. C. C.Mechanistic study of apatite formation on bioactive glass surface using 31P solid-state NMR spectroscopy, Chem. Mater. 2005, 17(17), 4493-4501.DOI: 10.1021/cm050654c
33. Bingöl, O. R,; Durucan, C. Hydrothermal synthesis of hydroxyl apatite from calcium sulphate hemihydrates, Am. J. Biomed. Sci. 2012, 4(1), 50-59.DOI: 10.5099/aj120100050
34. Peitl, O.; Zanotto, E. D.; La Torre, G. P.; Hench, L. L. Bioactive ceramics and method of preparing bioactive ceramics, Patent WO/1997/041079, November 06, 1997.
35. Peitl, O.; Zanotto, E.D.; Hench, L.L. Highly bioactive P_2O_5–Na_2O–CaO–SiO_2 glass-Ceramics, J. Non-Cryst. Solids 2001, 292(1-3), 115-126. DOI: 10.1016/S0022-3093(01)00822-5
36. Oliveira, J. M.; Correia, R. N.; Fernandes, M. H. Effects of Si speciation on the in vitro bioactivity of glasses. Biomaterials 2002, 23(2), 371-379. DOI: 10.1016/S0142-9612(01)00115-6
37. Clupper, D. C.; Mecholsky J. J. Jr.; LaTorre, G. P.; Greenspan, D. C. Sintering temperature effects on the in vitro bioactive response of tape cast and sintered bioactive glass–ceramic in Tris buffer, J. Biomed. Mater. Res. 2001, 57(4), 532-540. DOI: 10.1002/1097-4636(20011215)57:4<532::AID-JBM1199>3.0.CO;2-3
38. Hench, L. L.; Splinter, R. J.; Allen, W. C.; Greenlee, T. K. Bonding mechanisms at the interface of ceramic prosthetic materials, J. Biomed. Mater. Res. 1971, 5(6), 117-141. DOI: 10.1002/jbm.820050611

